eurizon
European network
for developing new horizons for RIs

Project information

Project full title	European network for developing new horizons for RIs
Project acronym	EURIZON
Grant agreement no.	871072
Instrument	Research and Innovation Action (RIA)
Duration	01/02/2020 – 31/01/2024
Website	https://www.eurizon-project.eu/

Deliverable information

Deliverable no.	D5.7
Deliverable title	Status report on R&D work on inner tracker for low energy electron-positron colliders
Deliverable responsible	
Related Work-Package/Task	WP5; Task 5.4
Type (e.g. Report; other)	
Author(s)	G. Bencivenni, G. Morello, E. De Lucia, R. Farinelli, M. Giovannetti, M. Poli Lener
Dissemination level	Public
Document Version	1.1
Date	21/12/2023
Download page	

Document information

Version no.	Date	Author(s)	Comment
1.0	18/12/2023	G. Bencivenni, G. Morello, E. De Lucia, R. Farinelli	
1.1	21/12/2023	G. Bencivenni, E. De Lucia	

Table of Contents

Development and Design of a Low Mass Modular Inner Tracker based on Cylindrical micro-RWELL Technology

The aim of this task is the development of a low mass modular Inner Tracker (IT) for low energy positron-electron colliders based on Cylindrical micro-RWELL (C-RWELL) technology, designed and built by the INFN-Ferrara and LNF collaboration.

1. The low-mass modular C-RWELL

The cylindrical-RWELL (C-RWELL) is a low material budget (O(1%) X_0) full cylindrical IT based on the μ-RWELL technology. The μ-RWELL [1,2] is a resistive Micro Pattern Gas Detector (MPGD) composed of two PCBs: a mono-layer PCB acting as the cathode, defining the gas detector gap, and a μ-RWELL_PCB that couples in a unique structure the electron amplification and the readout stages (Fig.1.1). A 50 μm thick polyimide foil, copper clad on the top side and sputtered with Diamond-Like-Carbon (DLC, [3]) on the opposite side, is coupled to a standard PCB readout board, through a 50 μm thick pre-preg foil. The thickness of the DLC layer (50÷100 nm) is adjusted according to the desired surface resistivity value (50÷100 MΩ/square) to provide discharge suppression as well as current evacuation. The spark suppression mechanism, intrinsic to the μ-RWELL technology, makes the operation of this detector safer with respect to other MPGDs. A chemical etching process of the polyimide foil is performed on the top surface of the overall structure to create a GEM (Gas Electron Multiplier)-like matrix of truncated cones with 70 μm (50 μm) top (bottom) diameter and 140 μm pitch. This pattern constitutes the amplification stage. The high voltage applied between the copper and the DLC layer produces the required electric field within the WELLs that is necessary to generate charge amplification (Fig. 1.2). The signal is capacitively induced on the strips/pads on the readout board. The introduction of the resistive layer allows to achieve large gas gains up to 10^4 with a single amplification stage, while partially reducing the capability to stand high particle fluxes. Thanks to the technological evolution of PCB manufacturing, leading to a reduced thickness and increased flexibility of the base material, it is possible to bend the μ-RWELL_PCB and achieve the unprecedented development of a cylindrical-RWELL. In addition, the detector is designed to be "openable" and "modular" such that in case of malfunctioning of any part, this piece can be easily replaced.
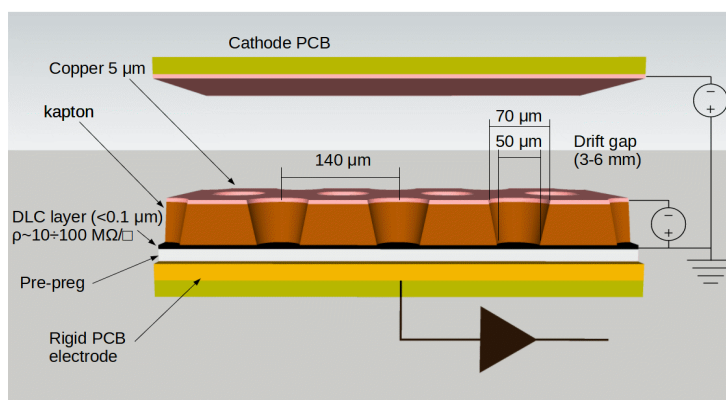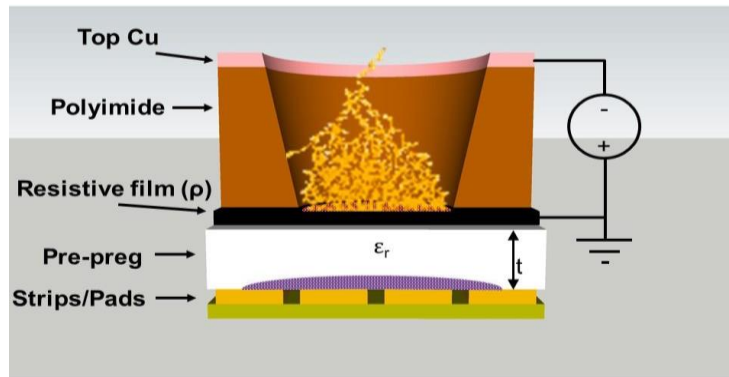

Fig.1.1: Basic layout of a μ-RWELL.

Fig.1.2: Principle of operation of the μ-RWELL.

The reconstruction of the particle track traversing the gas sensitive gaps will be based on a combination of two algorithms: Charge Centroid (CC) and μ-TPC. Tests performed with planar prototypes show that an almost uniform space resolution below 100 μm over a wide angular range of track incidence (0 ÷ 45°) is obtained [4]. As shown in Fig.1.3, at low drift fields the measured space resolution improves reaching values down to 65 μm.
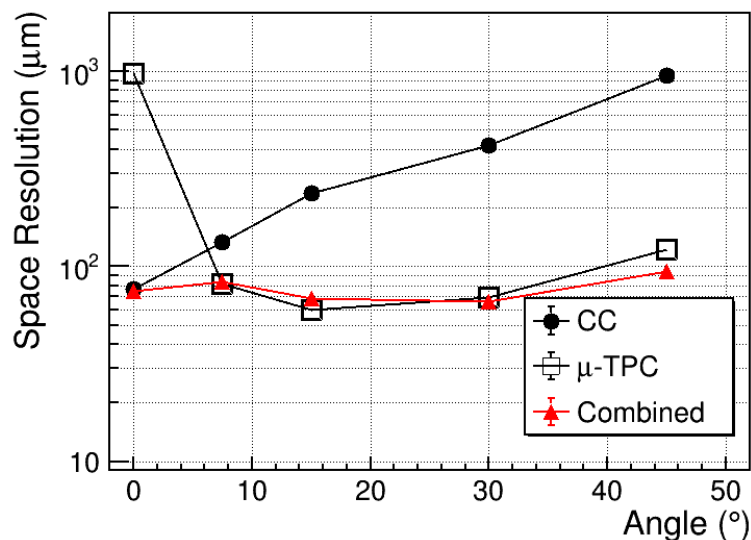

Fig.1.3: Comparison of the two algorithms with their combined reconstruction, at a drift field ED = 1kV/cm.

2. Design and construction of the C-RWELL components

The main feature of the μ-RWELL is to have the amplification stage, the resistive layer and the readout board embedded in a single element. The possibility to build this element with flexible substrates makes the technology suitable for non-planar geometry. Two ideas of a C-RWELL

have been studied, both based on a common double-faced cathode layout. In one case (Fig. 2.1 - left) a two large radial gaps option with 10 cm global sampling gas along the radial direction has been considered, while in the second case (Fig. 2.1 - right) four thinner gaps with 4 cm global sampling gas are foreseen. Depending on the material choice, the first layout could be done with a global material budget in the range $0.75 \div 0.86\%$ X_0, while the second in the range $1.46 \div 1.72\%$ X_0. For both layouts, the cylindrical μ-RWELL_PCB is divided in three "roof-tiles" shaped detectors that, thanks to the possibility to open (and re-close) the cylindrical support, are replaceable in case of malfunctioning.

A 1 cm large mono-gap prototype, composed of coaxial cylindrical anode and cathode structures, has been designed (Fig 2.2) and realized by LOSON S.r.l., a company with a well-established expertise in composite materials. The substrate for the electrodes is Millifoam. The dimensions and all relevant numbers of the prototype are summarized in Table 2.1.
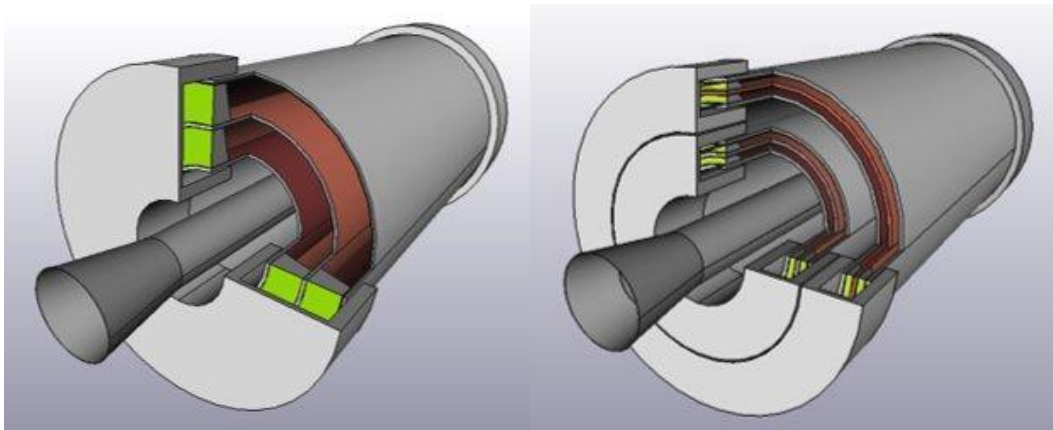

Fig.2.1: The two layouts for the Inner Tracker: on the left the double large gas gap; on the right a pair of double thinner gas gaps.
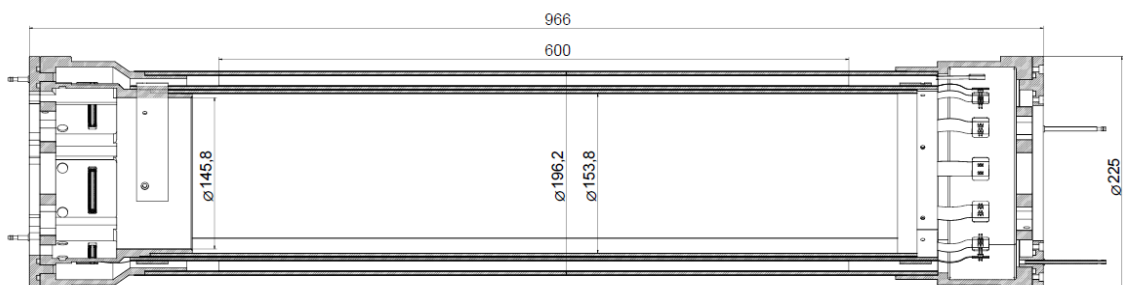

Fig. 2.2: Cross-section of the C-RWELL mono-gap prototype

Table 2.1: Dimensions (mm) and relevant numbers of the C-RWELL prototype.

anode dia.	cathode dia.	drift size	active length	# HV chs	# r/out chs	strip pitch
168.5	188.5	10	600	12	768	0.68

The cathode

The cathode is the outermost electrode of this prototype, it has been stratified starting from a kapton-copper foil (Fig. 2.3-left). The stratification has been continued with a skin of fiberglass (Fig. 2.3-right), a layer of Millifoam (Fig. 2.4), a second fiberglass skin and a copper layer operating as a Faraday cage. The Millifoam is a material that once coupled with epoxy-glue and skins of fibre-glass, becomes extremely robust. The flanges at the two edges of the cathode are made of PEEK (polyether ether ketone).
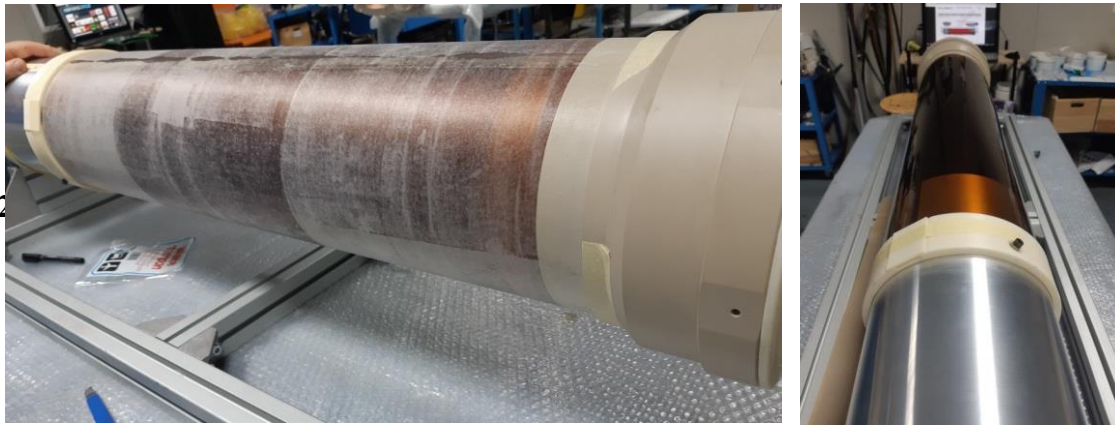

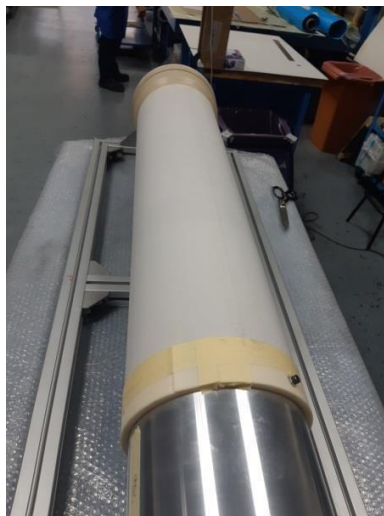Fig. 2.3: Cathode lamination: the initial copper layer (left) and the fiberglass deposition (right).

Fig. 2.4: Millifoam layer glued on cathode.

The anode

The cylindrical anode is composed of three roof-tiles, each with an angular coverage of 120° (Fig. 2.5). Each flexible μ-RWELL_PCB (Fig. 2.6), built at the CERN MPT Workshop, is equipped with axial strips, parallel to the axis of the cylinder. The roof-tile support of the μ-RWELL_PCB is made with a 3 mm thick Millifoam (Fig. 2.7), that is glued to the μ-RWELL_PCB.

The anode flanges, realized in PEEK, have been designed with proper windows to host the boards for the HV distribution (Fig. 2.8-left) and the interface boards for the connection of front-end electronics (Fig. 2.8-right). The presence of these openings has required a dedicated test for the gas tightness of the flange-boards system. The boards are glued to the inner surface of the flange with Araldite 2011. The gas tightness test has been performed with a dedicated tool (Fig. 2.9), where the system has been flushed with nitrogen, comparing the entering and the exiting gas flow; a second test has been done setting a 20 mbar over-pressure (condition much worse than the operating one, i.e. <5 mbar) inside the flange and monitoring the pressure drop as a function of time. The over-pressure decreased by about 1 mbar after 2 hours, then the test was stopped and considered successful. The construction of the prototype was completed in December 2021 (Fig. 2.10) and the final assembly of the detector was done in September 2023.

Fig. 2.5: Sketch of the assembly of the three roof-tile detectors on the anode cylinder. The anode cylinder is made of composite material: FR4 - Millifoam - FR4 sandwich plus an additional finely machined layer of Millifoam.

Fig. 2.6: Flexible μ-RWELL_PCB detector tiles manufactured at the CERN MPT Workshop.

3. C-RWELL prototype assembly

The final assembly of the C-RWELL, performed in a Clean Room (Class 1000), includes several phases hereafter listed and then described in detail:

1. Gluing the µ-RWELL circuit onto the Millifoam roof-tile
2. Curing cycle with vacuum bag technique
3. Assembling the detector roof-tiles onto the cylindrical anode structure
4. Soldering HV connections between roof-tile detectors and cathode
5. Inserting the anode structure within the cathode
6. Closing the detector
7. Installing HV distribution and filter PCBs, and FEE boards
8. Connecting the Faraday-cage

Step 1-2-3

The gluing of the µ-RWELL circuit onto the Millifoam tile involves several steps. A two-component Araldite 2011 epoxy-glue is distributed on a thin polypropylene foil (Fig. 3.1). Then the transfer foil is carefully positioned and pressed onto the Millifoam tile to distribute the glue on the tile surface (Fig. 3.2). This glue transfer method, developed during the construction of prior cylindrical detectors based on GEM technology [5,6], ensures precise and consistent glue deposition.
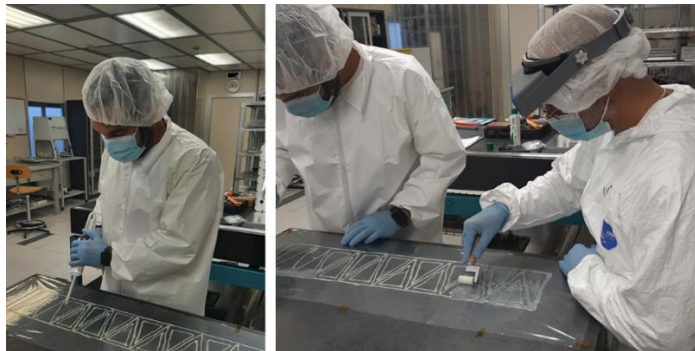

Fig. 3.1: Epoxy-glue disposal on the polypropylene foil (transfer technique).

Fig. 3.2: Transfer of the epoxy-glue from the polypropylene foil to the Millifoam roof tile.

The Millifoam tile is then placed onto the aluminum mold. The µ-RWELL circuit is accurately placed on the tile and centered with reference pins and counter-flanges (Fig. 3.3).

Fig. 3.3: An anode circuit after the glue curing cycle. Counter-flanges at the edges are visible in this picture (black and blue).

The whole gluing set-up is covered with a peel-ply sheet, ensuring a uniform distribution of the vacuum pressure over the components to be glued, and enclosed with a polypropylene vacuum-bag and sealed with a vacuum-proof mastic. An oil-free pump provides the vacuum (Fig. 3.4). After a 12-hour curing time, the vacuum-bag is opened, and the detector tile undergoes quality control using an insulation tester. Up to 500 V are applied to the amplification stage, ensuring a current of less than 1 nA. Each roof tile is fixed to the rectified anode structure using two PEEK arcs at the edges of the active area, housing the holes for two plastic screws (Fig. 3.5).
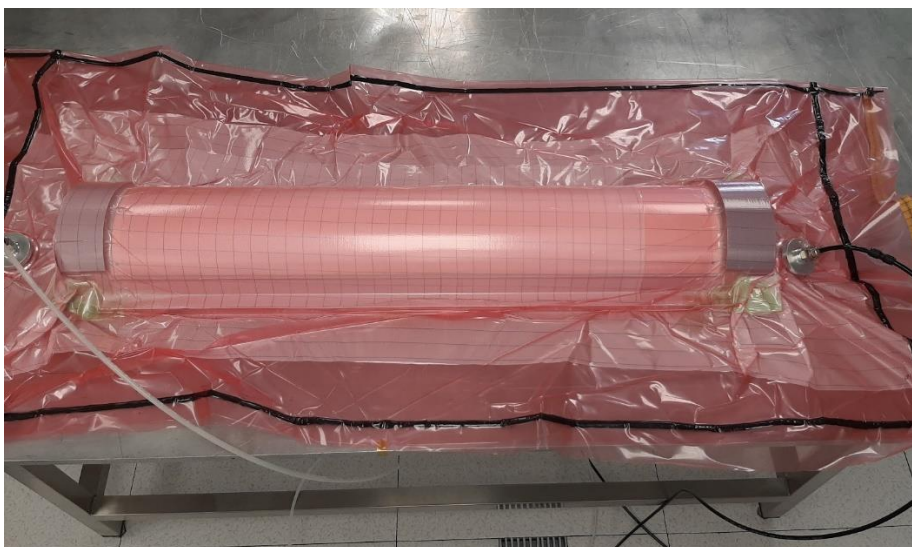

Fig. 3.4: The vacuum bag for the curing cycle of the Araldite 2011.

Fig. 3.5: The assembly of an anode roof-tile on the Millifoam structure.

Step 4

The electrodes are then equipped with HV connectors. The circuit receives power through tails plugged into a pair of two-pin connectors, with 2.54 mm pitch, leading to the HV interface boards attached to the flange.
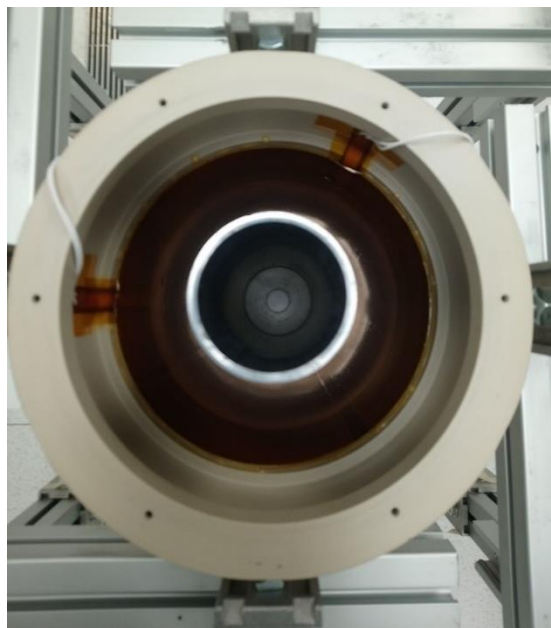

Fig. 3.6: the cathode equipped with the wires for the HV distribution. The aluminum tube for the final assembly is also visible.

The top of the amplification stage is connected to HV, while the resistive layer is grounded. To prevent misalignment among pins and plugs on the boards, connector soldering occurs when the cylindrical anode is in position, partially inserted into the cathode structure. The anode HV flange hosts the interface board for the cathode. A unipolar wire is soldered to each of the two cathode tails (Fig. 3.6) and then to the standard connector.

Step 5-6

Despite the 1 cm large gap between the inner cathode surface and the µ-RWELL, the insertion of the anode into the cylindrical cathode demands care. Any misalignment between the axis of the two cylinders can lead to friction and subsequent damage. It is therefore imperative to prevent cathode movements during the operation while ensuring the correct alignment of the two axes. The first requirement has been met exploiting the structure shown in Fig 2.10: a "cage" has been created with small aluminum profiles (Fig. 3.7-left) to encase and secure the cathode. A 1 m-long metallic tube has been installed along the axis of the cathode (Fig. 3.6) and fastened at the base to act as a guide for the anode. The anode has been equipped with a PET "cup" (Fig. 3.7 top-right), mounted on the innermost part of the readout flange, sliding along the aluminum tube. The coaxial alignment between the two electrodes is provided by the PEEK endcaps (Fig. 3.7 bottom-right), housing the gas connectors and O-rings for gas tightness. The two endcaps are fixed to the electrode flanges, completing the detector mechanical assembly (Fig. 3.8).
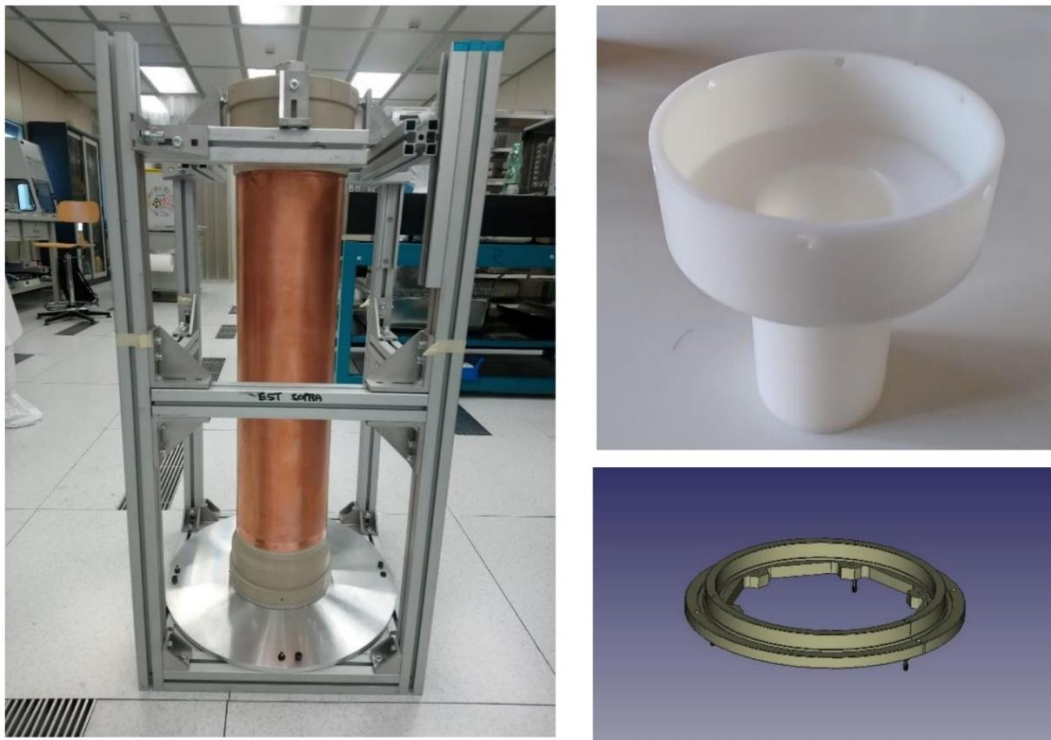

Fig. 3.7: Tools for the final assembly.

Fig. 3.8: The assembled detector

Step 7

The detector HV distribution is divided in three regions:

1. the connection of the circuit tails to the interface boards (described in the previous paragraph), inaccessible after detector assembly.

2. the connection of each interface board to the HV PCB divider (Fig. 3.9) through an RCR filter.

3. the connection of the HV PCB divider to the power supply.

The interface board is designed to host on the side facing the gas gap the pins soldered on the circuit tails, and on the other (Fig. 3.8) a small board with an RCR circuit. The HV PCB divider is fixed to the PEEK flange using six 50 mm-long spacers. The connection between the two boards is provided by a set of paired wires.
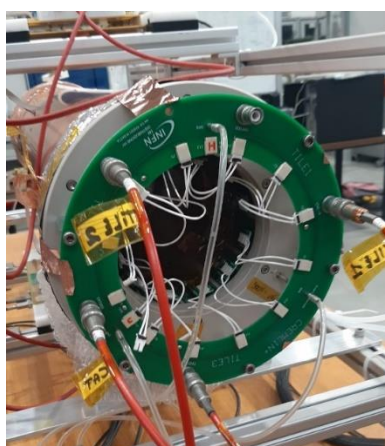

Fig. 3.9: The HV PCB divider.

The PCB divider hosts five Huber-Suhner connectors: three dedicated to the three roof-tiles, one for the cathode and the last one as a spare HV channel. The front-end boards, based on the APV25 ASIC, are plugged on the intermediate boards located on the dedicated flange. Each APV board is read-out by a HDMI cable transmitting signals to a Scalable Readout System (SRS) module [7].
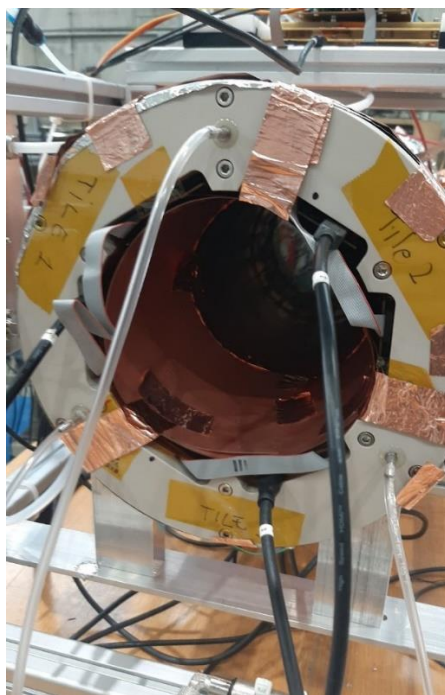

Fig.3.10: Shielding of the FEE side.

Step 8

The Faraday cage of the detector is composed of the innermost part of the anode, the outermost part of the cathode and the PCB divider. The innermost layer of the Faraday cage acts as reference grounding also for the front-end electronics (Fig.3.10): small copper strips have been soldered for this connection.

The total assembly of the detector took about one week.

4. Detector performance

The C-RWELL performance has been studied using a cosmic-ray stand equipped with an external tracking system (Fig. 4.1).

The detector has been operated with a 50 cc/min flux of $Ar/CO_2/CF_4$ (45:15:40) gas mixture. The TOP electrode, responsible for the µ-RWELL signal amplification, is set to values ranging between 550 V and 610 V and the DLC is always grounded. Drift field values between 0.5 and 4 kV/cm have been used. The measured dark current for each tile is less than 1 nA. The PCB divider hosts five Huber-Suhner connectors: three dedicated to the three roof-tiles, one for the cathode and the last one as a spare HV channel. The front-end boards, based on the APV25 ASIC, are plugged on the intermediate boards located on the dedicated flange. Each APV board is read-out by a HDMI cable transmitting signals to a Scalable Readout System (SRS) module [7].
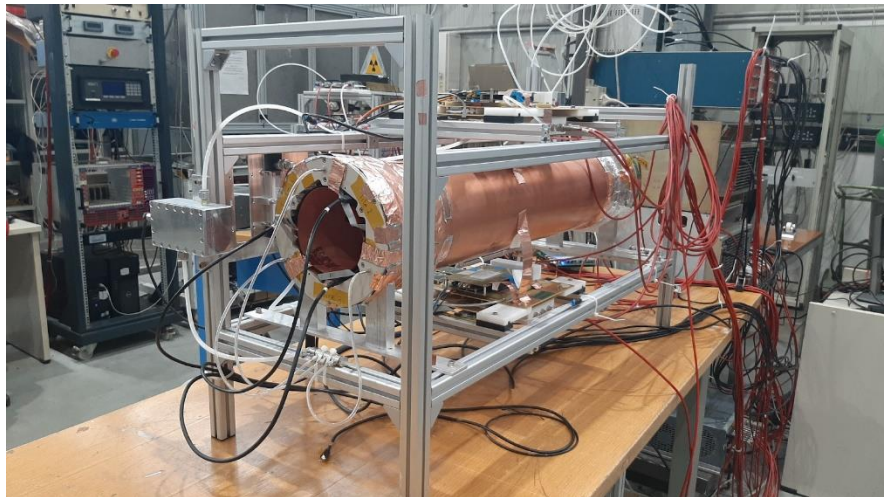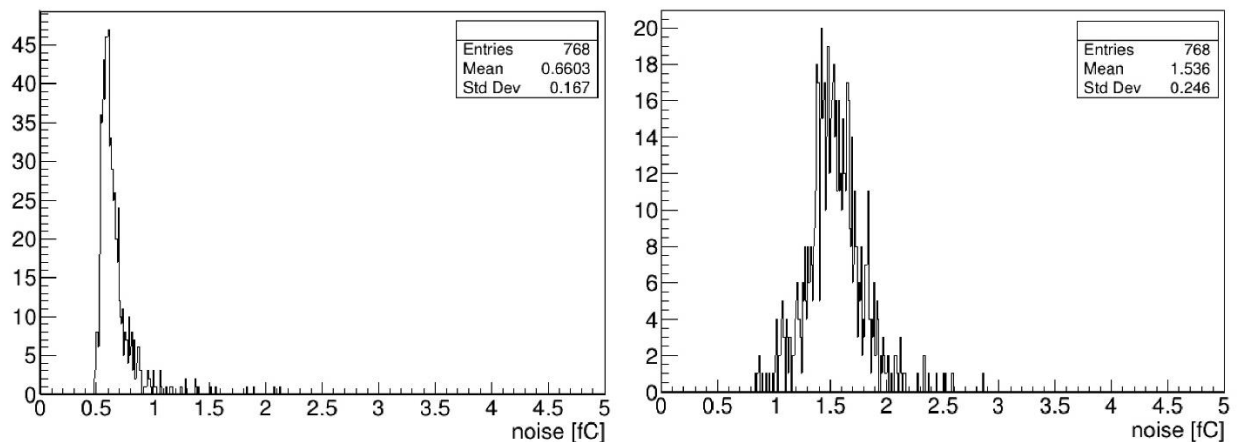

Fig. 4.1: The cosmic ray setup.

Fig. 4.2: Standard deviation of pedestals for all C-RWELL FEE channels: at the beginning of the data taking (left) and at the end (right).

Grounding and detector shielding optimization allowed an average noise level of approximately 0.7 fC to be reached (Fig. 4.2-left), even though at the end of the data taking the noise value increased up to 1.5 fC (Fig. 4.2-right).
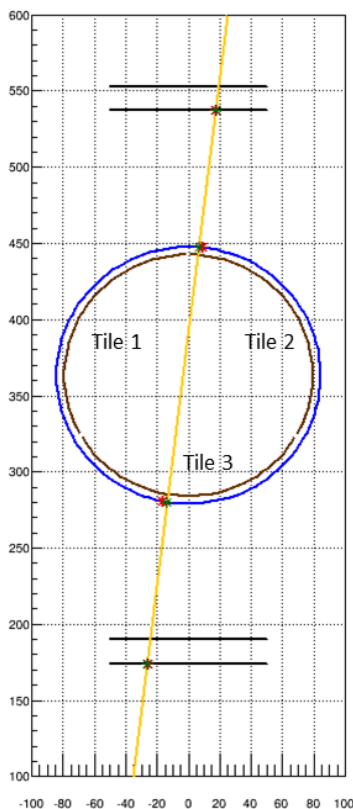

Fig. 4.3: A typical cosmic ray event (X coordinate on the horizontal axis and Z coordinate on the vertical one).

The trigger system is composed of two 8x8 cm^2 plastic scintillators. The external tracking system is composed of two sets of 10x10 cm^2 XY trackers, placed above and below the C-RWELL (Fig. 4.1) and defining the X-Y plane. The C-RWELL is equipped with a one-dimensional readout, with strips parallel to the ones of the X-trackers. Fig. 4.3 shows a reconstructed event display with the layout of the tiles on the r-phi (X-Z) plane seen from the FEE side. The reconstructed position in the middle of the drift gap (blue) is shown together with the position of the three tiles (brown). The gap between two contiguous tiles is about 3 mm, corresponding to an angle of 2°. In the analysis the C-RWELL is divided into a top and a bottom part. Taking into account the trigger geometrical acceptance, the top part is composed of tile 1 and 2, while the bottom part is tile 3.

The signal acquired from the trackers and the C-RWELL undergoes clusterization, the algorithm defining a set of contiguous strips as *cluster* and their multiplicity as *cluster size*. The position of the cluster is reconstructed using the Charge Centroid (CC) method. The tracking

system provides the reference for the C-RWELL, and it facilitates a clean event selection for the analysis. The event selection requirements for the trackers are:

- one single cluster reconstructed on each tracker.
- cluster size lower than 5.
- track angle below 3° w.r.t. the vertical axis.

Defining the Field Of Interest (FOI) as the region around the expected track position, extrapolated from the fit to the external trackers clusters, only C-RWELL events in the FOI of 1 cm are selected for the analysis.

From the data analysis the following quantities are measured: cluster size and charge, the efficiency, and the distribution of the residuals, defined as the distance between the expected and reconstructed clusters.

For each HV and drift field configuration, a total number of triggers between 20000 and 30000 has been collected, during about three days of data acquisition with the cosmic-ray setup. A test beam would be required for a better and faster detector response characterization. In order to define the working point of the detector, a drift field scan in the range 0.5 - 4 kV/cm has been performed with 600 V applied to the TOP electrode. Both the cluster charge and size have been measured (Fig. 4.4), with the cluster charge value extracted as the most probable value (MPV) of the Landau function fit to the cluster charge distribution.
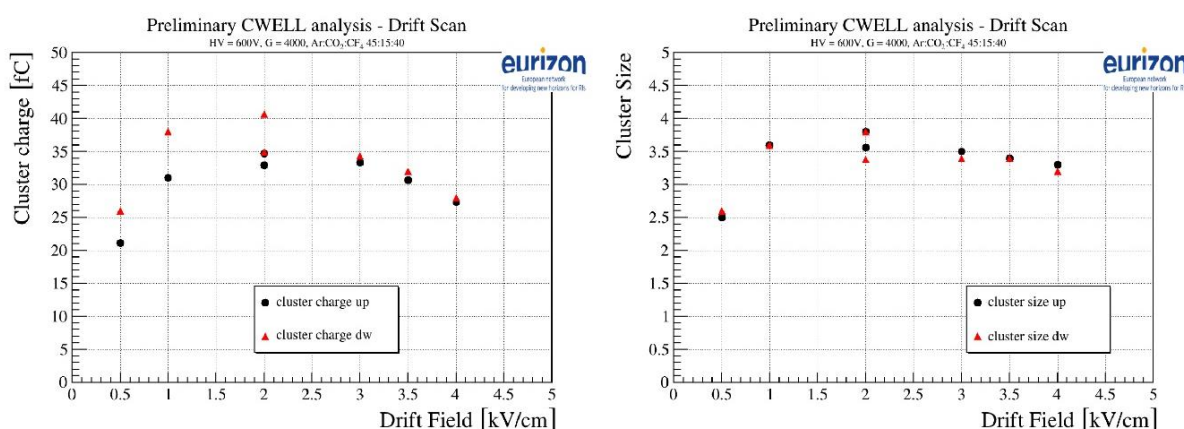

Fig. 4.4: Cluster charge (left) and cluster size (right) as a function of the drift field, for HV=600V.

The drift field plays a fundamental role in the collection of primary electrons. Optimizing this parameter is essential to enhance detector performance [1], and this is confirmed by the measurements reported in Fig. 4.4. Both cluster charge and size exhibit a maximum value at a drift field around 2 kV/cm and lower values at lower drift fields can be explained by the recombination of primary ionization electrons. At higher drift field values, the defocusing effect of the field lines leads some primary electrons to be collected on the top copper without being multiplied [8]. A second scan has been performed changing the HV settings from 550 V to 610 V while keeping the drift field value at 2 kV/cm. Fig. 4.5 shows the cluster size and charge as a function of the HV value applied.
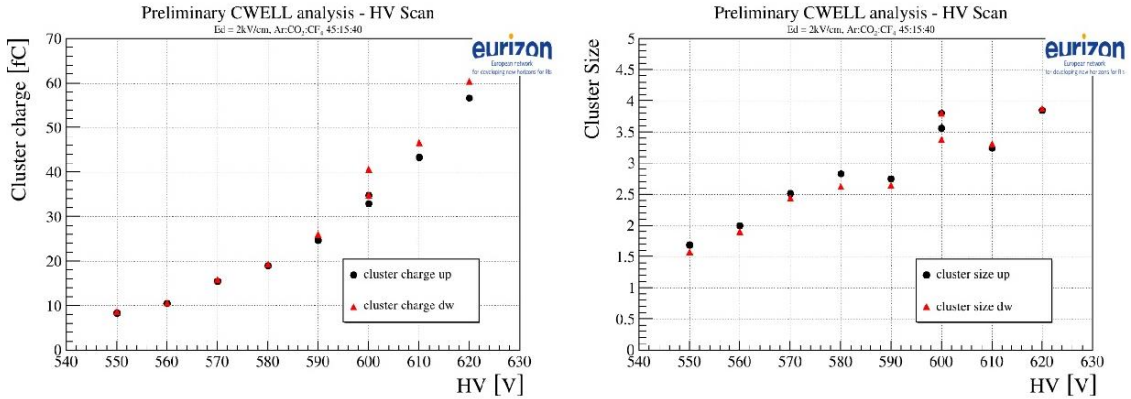
Fig 4.5: Cluster charge (left) and cluster size (right) as a function of the HV on the TOP electrode for a drift field of 2 kV/cm.

The cluster size increases, as expected, with the HV as well as the charge per cluster. The different behavior of the points in Fig. 4.5-right depends mainly on the FEE thresholds used. The points at HV = 590 V and 610 V have a threshold 2 times larger than the other HV values and the cluster size suffers mainly from this parameter.
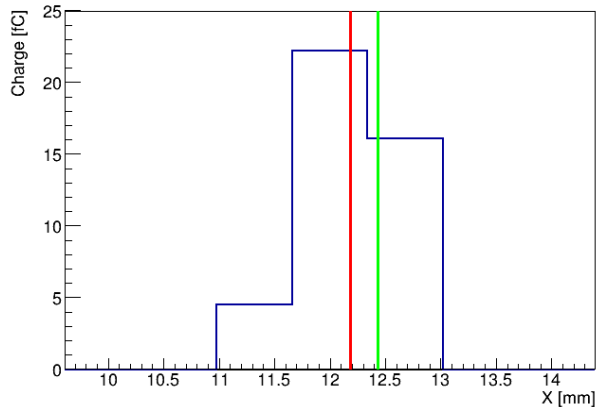

Fig. 4.6: Reconstructed event: the blue line shows the charge collected on three contiguous fired strips; the red line is the reconstructed position, while the green line is the expected one.

The fit to the residuals distribution of the C-RWELL (Fig. 4.7) with a Gaussian function, gives a width of about 460 µm. This value, besides the intrinsic space resolution of the detector, includes also the contribution from the tracking system and the effect of the impinging angle of the particles (as shown in Fig. 1.3). The width of the residuals distribution as a function of the HV value is shown in Fig. 4.8. A test beam campaign would be required to disentangle the detector space resolution from the contributions above mentioned. The efficiency plateau for the top and bottom parts of the C-RWELL is 90% and 96% respectively (Fig. 4.9). The lower value of the efficiency of the top part is expected and due to the presence of a 3 mm dead zone between the tiles.
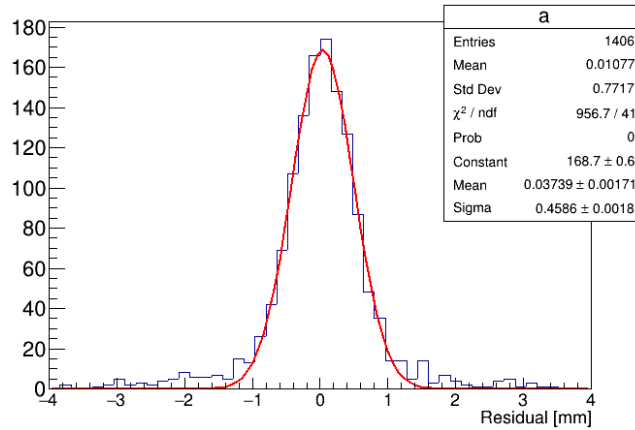
Fig 4.7: Residual distribution with the Gaussian function fit at HV = 600 V and drift field = 2 kV/cm for the bottom part of the C-RWELL.
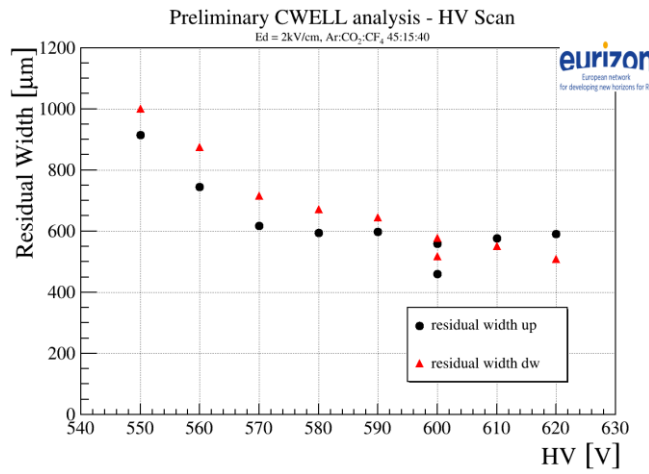

Fig. 4.8: Residuals width as a function of the HV for the top and bottom part of the C-RWELL.
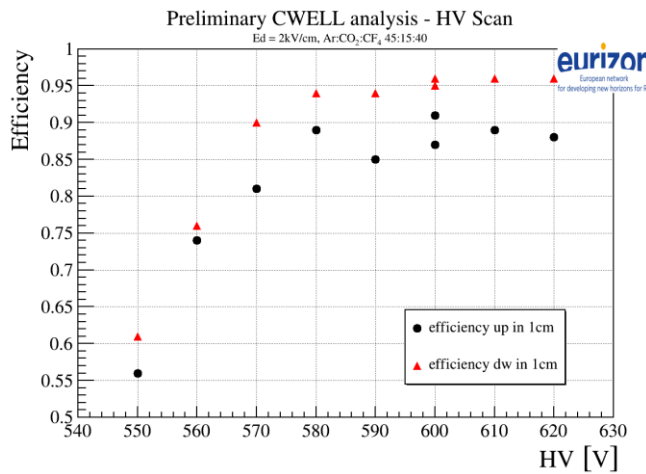

Fig. 4.9: Efficiency as a function of the HV for the top and bottom part of the C-RWELL.

5. Detector simulation

The software framework based on Gaudi, is a key element of the project. The implemented strategy for the C-RWELL software tools starts with the geometry description, using DD4HEP, the simulation of energy deposition and detector response, and the digitization stage. For the detector response parameterization, a fast simulation has been developed starting from a dedicated simulation software used for BESIII triple-GEM detector [9] and adapting it to the μ-RWELL detector with the aim of simulating the resistive stage and validating it with DATA/MC matching of known planar detector configuration studied at test beams. To this extent during October 2021 a test beam has been performed at CERN H8 area with planar μ-RWELL detectors built with different values of DLC resistivity.

The software strategy and implementation will be described together with preliminary results obtained with the C-RWELL detector simulation and the dedicated detector response parametrization.

Geometry description

For the time being the geometry of the second option for the C-RWELL detector (see Fig. 2.1 - right) has been implemented using DD4HEP. In this case four small gaps with 4 cm global sampling gas are foreseen. As for the materials and cathode and anode details, the mechanical drawings and description have been used. The new materials characterizing the detector have been inserted in the sub-detectors material listing: FR4, DLC and so far honeycomb. Detector sensitive layers and materials have been defined to allow hits generation to be performed. Figure 5.1 shows the first results from the full detector simulation: on the left the 3D distribution of Geant4 hits generated and saved in the C-RWELL detector with 100 MeV pions from ParticleGun with $75 < \text{theta} < 105$ degrees and $0 < \text{phi} < 360$ degrees. Figure 5.1-right shows the comparison between the distribution of the number of hits in the C-RWELL detector obtained with 50 MeV pions in red and with 100 MeV pions in blue respectively. This is part of the soft pion study aiming at the evaluation of the vertex reconstruction efficiency and resolution for pions with momentum $p < 100$ MeV.
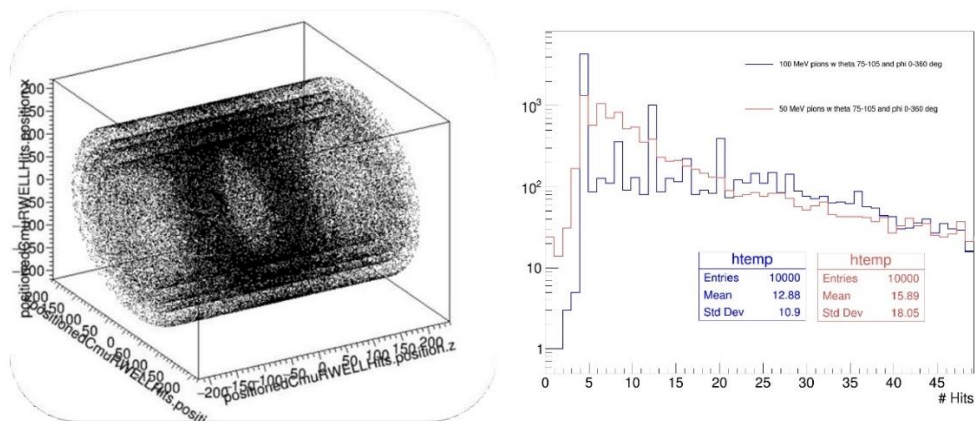

Fig. 5.1: 3D distribution of hits in C-RWELL from 100 MeV pions (left) and the number of hits in C-RWELL obtained with 50 MeV pions in red and 100 MeV pions in blue (right).

Digitization

The complete simulation of the C-RWELL includes also the response of the detector to the energy deposition, with the description of the formation of the electronic signal inside the detector. The output of the digitisation is the raw hit, which in the case of the C-RWELL consists in the charge and time measurements associated with the fired strip. From this raw information the position where the particle passed inside the detector volume can be reconstructed and used in track finding and track fitting algorithms.

The response of the detector can be modeled with different levels of approximation.

A C-RWELL digitization package has been implemented in the Aurora framework. Currently it hosts a simplified digitization procedure, which skips the full description of the physics inside the detector and simply transforms the Monte Carlo (MC) point from Geant4 directly into a reconstructed hit. The reconstructed hit contains the information on the position, which is computed at the center of the drift gap, starting from the MC entrance and exit points obtained by Geant4, with an additional smearing which accounts for the expected position resolution (see Fig. 5.2). Additionally, the reconstructed hit provides the measured charge, computed starting from the total energy deposit from the MC, and the signal time, calculated as the average value of the time associated to each MC point.
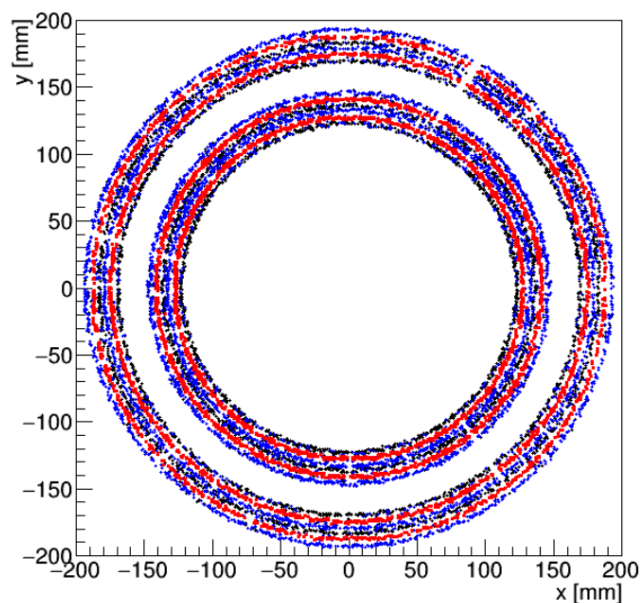

Fig. 5.2: Transverse view of the MC entrance (black) and exit (blue) points in the gas gaps. The digitized hits are drawn in red and are at the center of the gas gap. One thousand positive pions with momentum 200 MeV/c have been simulated.

Detector Response Parametrization

The full digitization is under development in a standalone code. It takes into account the various physics processes that play a role in the raw hit formation. It is composed of several steps, one for each independent physics effect.

The production of primary and secondary ionization in the gas gap is simulated following Poisson statistics, the detector gain is reproduced by sampling from the Polya distribution, the effect of the material (and possibly of the magnetic field) is considered in the description of the electron drift with a proper treatment of the transverse and longitudinal diffusion effects. The actual formation of the signal on the anodic strip is then simulated, by taking into account the induction of the current, the presence of the resistive plane and the applied electronics. The digitization standalone code is borrowed from the BESIII CGEM-IT project [9]: each step of the digitization is firstly studied by dedicated GARFIELD++ [10] runs, from which the parameters are extracted and used to describe the physics effect under study in a simplified, fast, parametrized way. The effect of the resistive layer, which is present in the μ-RWELL but not in the GEM technology, has been additionally implemented. The charge density spread on the resistive layer has been described in [11,12]. The model has been adapted to a one-dimensional readout. The charge density spread depends on the charge produced in an avalanche, on its space and time distribution when entering the WELL and on the parameter called τ, i.e. the decay time of the charge density due to the electrons movement towards the ground on the resistive surface. The effect of the APV25 electronics is inserted in the simulation by its response function convoluted with the charge density spread.
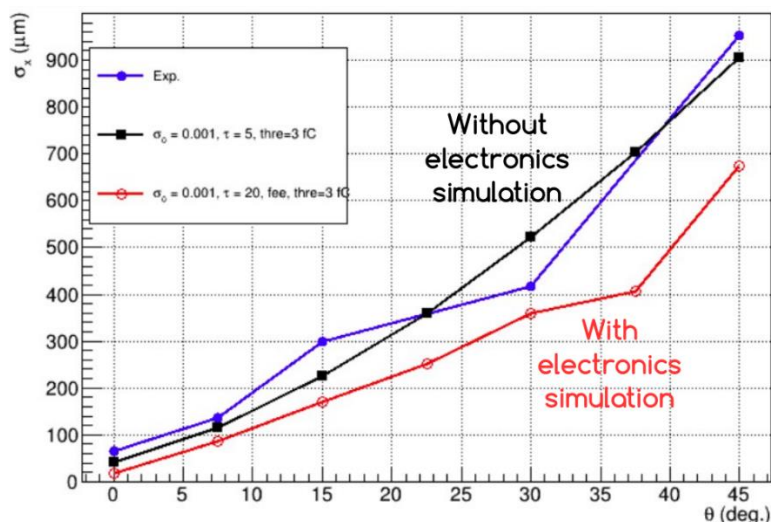

Fig. 5.3: Sigma of the charge spread distribution as a function of the track incident angle, simulated with (red) and without (black) the simulation of the electronics and extracted from experimental data (blue).

A preliminary evaluation of the sigma of the resulting distribution is shown in Fig. 5.3, where the sigma of the position residual distribution as a function of the track incident angle is reported. The residual is computed as the difference of the position reconstructed via the CC method and the MC point position. The black and red graphs are the simulation without and with the electronics simulation applied. Two different values of the τ time have been used. The τ parameter will be the object of a fine tuning of the simulated data onto the experimental ones. Nevertheless, there is already a remarkable accordance between the simulated and real results. A refined tuning procedure of the response simulation with experimental data is foreseen to properly reproduce the real detector performance. To this end, four sentinel variables have been

identified that fully characterize the C-RWELL behavior: cluster size, cluster charge, position resolution obtained with the CC and with the μTPC algorithms. The parameters of the simulation which need to be tuned are the τ time constant associated with the resistive plane and the threshold applied at the readout channel, to have a satisfactory match of the simulated sentinel variables and the values extracted by the experimental data.

Conclusions

This project successfully validated the concept of a low-mass inner tracker for low-energy positron-electron colliders based on full cylindrical micro-RWELL technology.

In comparison with cylindrical GEM, the C-RWELL, besides its intrinsic robustness exhibits several advantages such as the possibility to create a modular and openable detector, along with construction simplicity. The technology has been demonstrated to be easily adapted to non-planar geometries, serving as a proof of concept.

The collaboration with Loson Srl has led to the creation of lightweight and robust composite structures. The detector was assembled in September 2023 at LNF in approximately one week. Preliminary results obtained with cosmic-ray muons are very promising: the efficiency is up to 97%, while a first estimate of the space resolution is around 400 µm. However, it is worth noting that this is limited by the contribution from the tracking system and the effect of the impinging angle of the cosmic muons. A more accurate evaluation of the detector performance requires a test beam.

The geometry of the detector has been implemented in the DD4HEP framework. An innovative aspect of this task is the introduction of the resistive layer responsible for charge spread and, consequently, a larger cluster size. This work shows promise even at a very preliminary stage.

References

[1] G. Bencivenni et al., The micro-Resistive WELL detector: a compact spark-protected single amplification-stage MPGD, JINST 10 (2015) P02008.

[2] G. Bencivenni et al., The μ-RWELL layouts for high particle rate, JINST 14 (2019) P05014.

[3] A. Ochi et al., Carbon sputtering Technology for MPDG detectors, Proceeding of Science (TIPP2014) 351.

[4] G. Bencivenni et al., On the space resolution of the μ-RWELL, JINST 16 (2020) P08036.

[5] A. Balla et al., The cylindrical GEM detector for the KLOE-2 Inner Tracker, JINST 9 (2014) C01014.

[6] I. Balossino et al., The CGEM-IT: An Upgrade for the BESIII Experiment, Symmetry 2022, 14(5), 905.

[7] S. Martoiu, Development of the scalable readout system for micro-pattern gas detectors and other applications, JINST 8 (2013) C03015.

[8] S. Backmann et al., Charge amplification and transfer processes in the gas electron multiplier, Nucl. Instrum. Meth. A 438 (1999) 376-408.

[9] A. Amoroso et al., PARSIFAL: a toolkit for triple-GEM parameterized simulation, arXiv:2005.04452

[10] https://garfieldpp.web.cern.ch/garfieldpp/

[11] M. S. Dixit et al., Position sensing from charge dispersion in micropattern gas detectors with a resistive anode, Nucl. Instrum. Meth. A 518 (2004) 721-727.

[12] M. S. Dixit and A. Rankin, Simulating the charge dispersion phenomena in Micro Pattern Gas Detectors with a resistive anode, Nucl. Instrum. Meth. A 566 (2006) 281-285.